CLASSIFICATION OF HYPERSPECTRAL AND LIDAR WITH DEEP ROTATION FOREST

Junshi Xia and Zuheng Ming

[1] RIKEN Center for Advanced Intelligence Project (AIP), RIKEN, Tokyo 103-0027, Japan
[2] Laboratoire Informatique, Image et Interaction (L3i), University of La Rochelle, La Rochelle, France

ABSTRACT

In this work, a novel deep rotation forest is proposed to fuse hyperspectral (HS) and LiDAR. First, we extract the spatial and elevation information of two datasets by using morphological filters. Then, each feature source is applied to superpixel segmentation and then are treated as the input of deep rotation forest. In the deep rotation forest, the spatial relationships are fully considered, and the output probability of each layer is used as the input of the next layer. Experimental results demonstrate that the excellent performance of the proposed method.

***Index Terms*—** Deep rotation forest, classification, hyperspectral, LiDAR

1. INTRODUCTION

The recent remote sensing sensors and technologies brings us an opportunity to better understanding the objects of the earth from different views [1–6]. For instance, hyperspectral distinguishes the objects using the detailed spectral information [7], whereas light detection and ranging (LiDAR) separates the objects using the height information [8].

The effectiveness of the combination use of hyperspectral and LiDAR have been proved in the literature [1, 3, 4, 6]. Recently, few attentions have been paid to the joint use of multiple sources remote sensing datasets. For instance, Ghamisi *et al.* [9] proposed to use deep convolutional neural networks (DCNN) and extinction profiles (EPs) for the classification of HS and LiDAR. Multiple-level deep learning was used to classify crop areas with multi-temporal images [10].

Deep learning has been proved powerful in many fields [11, 12], however, they suffer to the following limitations [13]:

- they need a large number of training samples;
- they have many parameters that need to be tuned;
- they lacks theoretical explanation.

In order to alleviate the mentioned-above problems, we have proposed to use deep forest [14], which consists of the cascade structure of random forest and rotation forest [15]. Our studies indicated that deep forest is a good alternative to the deep neural network with fewer tuning parameters and short computational time.

In our previous work, we just use the stack morphological features as the input of the deep forest. We do not consider the spatial information in the construction of deep forest. In this paper, we introduce the superpixel segmentation [16] to consider the neighboring pixels and then formulate the spatial information into deep forest. We fully exploit rotation forest for the construction of deep forest.

This study has been carried out with financial support from RIKEN Center for Advanced Intelligence Project (AIP).

2. HYPERSPECTRAL AND LIDAR DATASETS

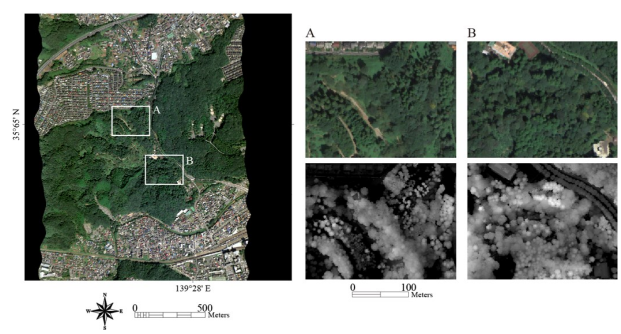

Fig. 1. (Left) RGB composite of HS in the whole area . (Right) RGB composite of HS and LiDAR @study areas (A) and (B).

In this work, a mixed forest area, called Tama Forest Science Garden, is chosen as the study area (seen in Fig. 1). HS image was obtained from CASI-3 sensor (72 bands) and LiDAR was acquired by LMS-Q560 (Riegel). We use the difference between DEM and digital surface model (DSM) as the feature of LiDAR. Both the datasets are re-sampled to 1 m [4].

Morphological openings and closings with partial reconstruction are used to extract features of both HS and LiDAR. For the HS data, the first three PCs are used [17]. Linear and disk-shaped structuring elements (SE) are adopted. The openings or closings over every 10° and use 10% of the length of the linear SE is adopted with the range of 5-10 and step size of 5. Thus, 20 opening and closings are obtained. For a disk-

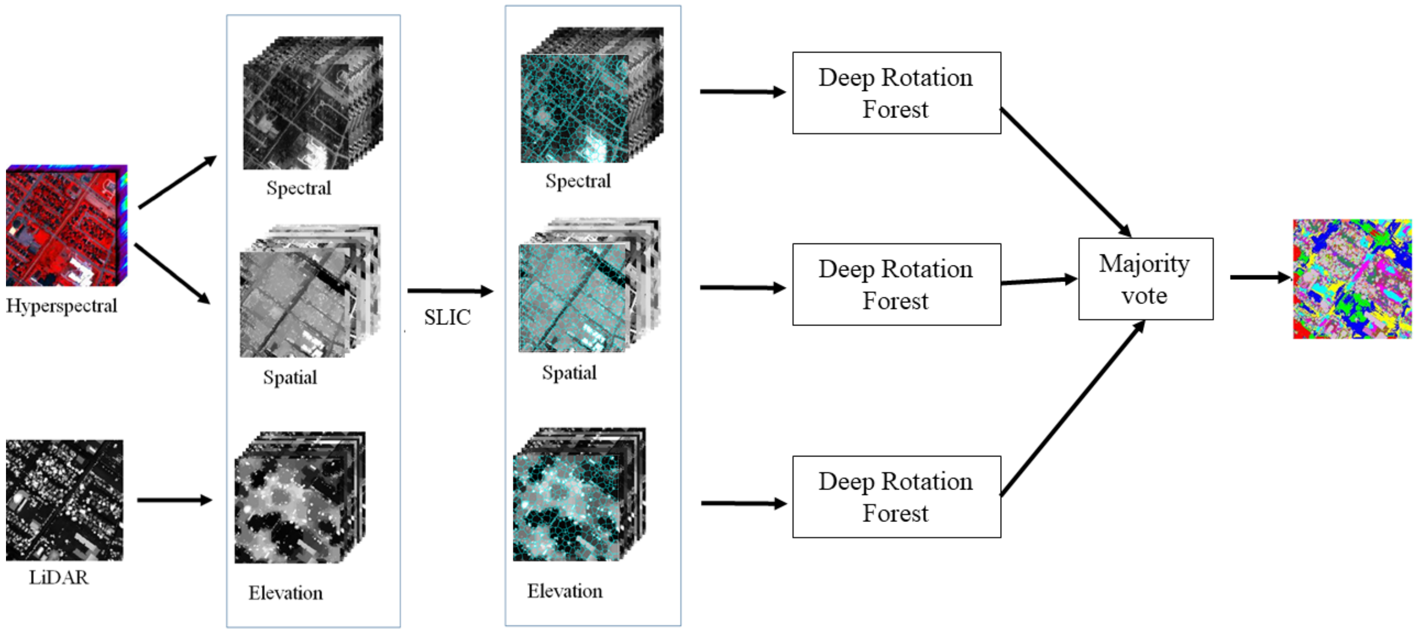

Fig. 2. The pipeline of our proposed approach.

shaped SE, the range is set to be from 1 to 15 with a step size of 1. Then, we can obtain 15 opening and closing.

Kernel principal component analysis (KPCA) [18] is used to make the same dimensions of three kinds of features (spectral, spatial and elevation) and reduce the noise. Finally, three kinds of features have the same dimensions (70).

3. OUR APPROACH

Our approach starts with a simple linear iterative cluster (SLIC) superpixels. We first train a rotation forest to learn the features among neighboring superpixels, and then directly input them to the classification stage to produce the class probabilities. Then, the average class probabilities and the original features are used as the input of the next layer. In the following, we details our approach with superpixel generation and deep rotation forest (seen Fig.2).

3.1. Superpixel generation

SLIC method can be treated as the extension of K-means applied to the feature space, which both consider the color and spatial information of each pixel. The size and the regularity of superpixels are controlled by one specific parameter. The computational speed is high, and the boundary properties are well maintained, so they make it possible to improve efficiency and generalizable to multiple features [16].

In this work, SLIC superpixels are computed using all the features of each source. The parameters in SLIC are empirically determined.

3.2. Deep rotation forest

Rotation forest aims at building various decision trees (DT) based on random feature selection and data transformation [19, 20]. More specifically, the feature space of original training set ($\mathbf{X}$) is randomly divided into K subsets ($\mathbf{X}_j, j = 1, 2, ..., K$) with the dimension of M. Then, in each subset, we select 75% size of the original training set and unitize PCA to obtain the coefficients: $v_j^1, ..., v_j^M$. A rotation matrix $\mathbf{R}$ is constructed as:

$$\mathbf{R} = \begin{bmatrix} v_1^1, ..., v_1^M & 0 & \cdots & 0 \\ 0 & v_2^1, ..., v_2^M & \cdots & 0 \\ \vdots & \vdots & \ddots & \vdots \\ 0 & 0 & \cdots & v_K^1, ..., v_K^M \end{bmatrix}$$

$\mathbf{R}$ is rearranged to $\mathbf{R}^a$ to make the same order to the original features. The new features are obtained by $\mathbf{XR}^a$. The above steps is repeated several times to obtain multiple new features.

The deep forest model adapts the cascade structure of many layers and each layer includes many decision forests.

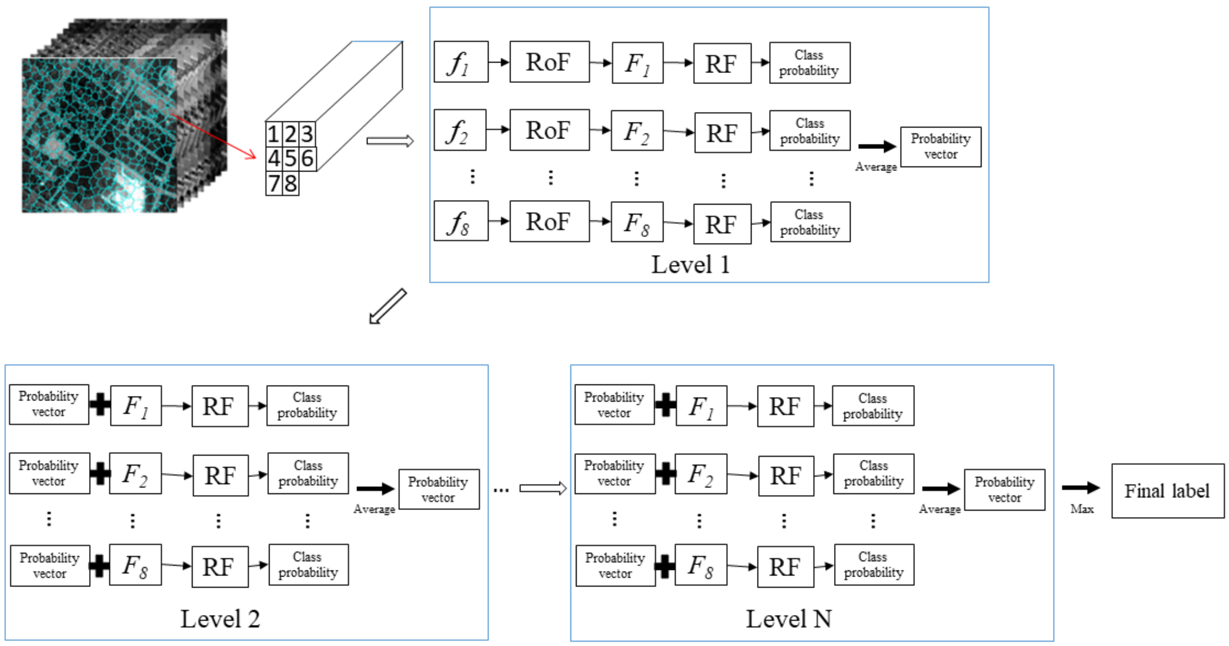

Fig. 3. Illustration of deep rotation forest (8 pixels in a patch).

In this work, the output of all former layers is used as the inputs of current layer. The output is used for the training for all following layers. The framework of the deep rotation forest is shown in Fig. 3.

As shown in Fig. 3, the superpixels of training samples are used for the training to include the spatial information. Just taking one patch (8 pixels) as an example, in the first level, the features (f_i) of each training sample with its neighborhood pixels are treated as the input of the rotation forest. Each rotation forest will produce the new features (F_i) with the same dimension of the original input features. Then, the new features are fed into a random forest to generate classification probability. The robust feature vectors can be obtained by the average of the above classification probabilities. The average classification probabilities and the new features extracted by the rotation forests are combined for the training features of next level. It should be pointed out that the averaged classification probabilities are used for all subsequent levels. Finally, the label is predicated with the maximum value from the classification probabilities of last level.

In our model, we apply deep rotation forest to the three feature sources: spectral and MPs of HS and MPs of LiDAR, respectively. The final classification result is obtained by their combination outputs.

4. RESULTS AND ANALYSIS

In the deep rotation forest, we set the number of DTs in RF and RoF to 10. The number of features in a subset (M) is set to be 10. 10% samples are randomly chosen from the reference as the training set. The remaining are used for the testing. The following methods are used to compare with our proposed approach:

- the original HS (Ori$_{HS}$) with RF classifier;
- the MPs of the original HS (MPs$_{HS}$) with RF classifier;
- the MPs of the LiDAR (MPs$_{Li}$) with RF classifier;
- the stacked MPs of HS and LiDAR (MPs$_{HSLi}$) with RF classifier;
- the stacked features (Stack) with RF classifier;
- the stacked features with DCNN classifier [21];
- the stacked features with Deep forest (DF) classifier [15];

To make a fair comparison with the deep forest in our previous study [15], we list the classification results of deep rotation forest (1 level). Table 1 shows the accuracy values. The classification maps are illustrated in Fig. 4. From Table 1, the accuracies are low with single feature source (e.g., Ori$_{HS}$). Higher accuracies can be achieved by integrating

Table 1. Classification accuracies obtained from different schemes.

Class	Number Train	Number Test	Ori$_{HS}$	MPs$_{HS}$	MPs$_{Li}$	MPs$_{HSLi}$	Stack	DCNN	DF	DRoF
California incense cedar	30	304	19.08	54.93	65.13	61.18	62.17	82.24	78.29	**85.52**
Bald cypress	93	927	59.12	89.75	88.24	90.18	91.26	**96.12**	94.39	95.79
Japanese cypress	300	2995	74.52	86.38	86.58	89.25	90.18	91.92	91.79	**93.89**
Japanese cedar	350	3492	81.16	90.26	89.58	93.93	93.70	94.73	**97.19**	97.11
Deodar cedar	83	833	66.51	95.20	86.31	93.88	95.92	97.12	97.96	**98.08**
Loblolly pine	33	332	25.30	79.82	71.69	81.63	84.34	82.83	90.96	**93.37**
Eastern white pine	58	579	66.32	92.57	95.68	90.67	95.68	97.41	98.45	**98.79**
Koyama's sqruce	27	267	20.60	70.04	86.89	77.53	78.65	89.14	95.13	**97.38**
Momi fir	110	1095	67.14	73.61	68.04	74.98	78.54	86.39	85.11	**91.32**
American sweetgum	102	1019	63.30	94.50	93.72	95.29	94.11	89.60	**95.19**	**95.19**
Japanese bigleaf magnolia	76	762	44.36	64.57	69.29	67.72	71.78	77.03	79.53	**81.36**
Painted maple	76	755	37.18	84.11	74.16	80.66	83.31	83.18	82.78	**85.30**
Oriental raisin tree	36	361	37.67	81.72	86.98	82.83	84.21	85.60	**91.69**	90.02
Chinese evergreen oak	120	1204	36.71	80.56	76.25	77.82	82.89	81.48	86.46	**90.19**
Japanese blue oak	151	1505	41.26	81.00	71.56	83.06	86.38	80.53	89.57	**90.70**
Japanese blue oak	176	1755	61.08	81.77	82.45	85.01	84.33	84.56	90.60	**92.88**
OA			59.09	84.32	82.72	85.80	87.43	88.51	91.51	**93.24**
AA			48.57	81.30	80.93	82.74	84.78	87.38	90.32	**92.30**
κ			53.94	82.54	80.74	84.16	85.99	87.18	90.53	**91.46**

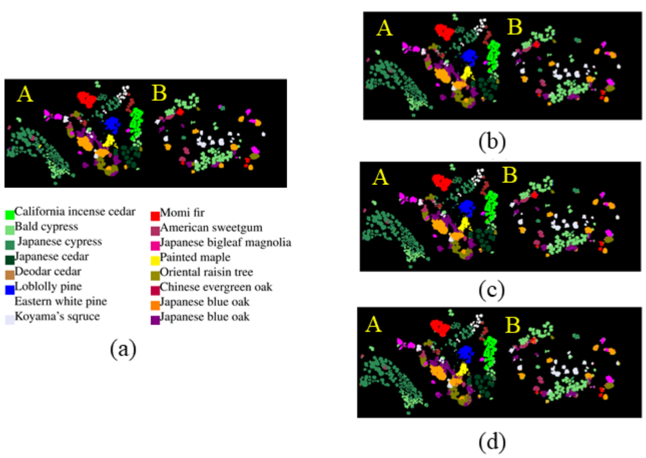

Fig. 4. (a) Ground truth. Classification maps of (b) DCNN. (c) Deep Forest. (d) Deep Rotation Forest.

multiple feature sources (e.g., MPs$_{HSLi}$ and Stack). Compared to DCNN and DF, the proposed deep rotation forest yields the best performance. The OA and AA are 93.24% and 92.30%, with the improvements of 2-3% than the ones of DCNN and DF. DRoF also shows the best results in twelve individual classes. Additionally, DRoF is efficient than DCNN.

Fig. 5 shows the sensitivity analysis of the number of levels. For the deep forest, when the number of levels exceeds three, the performance decreases. For the DRoF, the accuracies significantly increase and become stable after four levels.

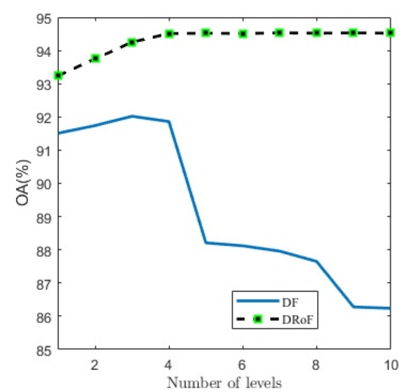

Fig. 5. Sensitivity analysis of number of levels.

5. CONCLUSION

In this work, a classification framework of hyperspectral and LiDAR with deep rotation forest is developed. We consider three kinds of features: spectral features of HS, MPs of HS and MPs of LiDAR. The final result is integrated by the results achieved by each feature source with the deep rotation forest. To incorporate spatial information, SLIC is introduced into the deep rotation forest. The proposed method obtains competitive performances.

6. ACKNOWLEDGMENT

The authors would like to thank Japan Space Systems (JSS) for providing the dataset.

7. REFERENCES

[1] M. Dalponte, L. Bruzzone, and D. Gianelle, "Fusion of hyperspectral and LiDAR remote sensing data for classification of complex forest areas," *IEEE Trans. Geosci. Remote Sens.*, vol. 46, no. 5, pp. 1416–1427, May 2008.

[2] D. Lemp and U. Weidner, "Improvements of roof surface classification using hyperspectral and laser scanning data," in *Proc. ISPRS Joint Conf- 3rd Int. Symp. Remote Sens. Data Fusion Over URBAN Areas5th Int. Symp. URS Areas, Tempe, AZ, USA, Mar 14-16*, 2005.

[3] M. Pedergnana, P. R. Marpu, M. Dalla Mura, J. A. Benediktsson, and L. Bruzzone, "Classification of remote sensing optical and LiDAR data using extended attribute profiles," *IEEE J. Sel. Top. Sign. Proces.*, vol. 6, no. 7, pp. 856–865, Nov 2012.

[4] T. Matsuki, N. Yokoya, and A. Iwasaki, "Hyperspectral tree species classification of Japanese complex mixed forest with the aid of LiDAR data,," *IEEE J. Sel. Topics Appl. Earth Observ. Remote Sens.*, vol. 8, no. 5, pp. 2177–2187, May 2015.

[5] Y. Gu, Q. Wang, X. Jia, and J. A. Benediktsson, "A novel MKL model of integrating LiDAR data and MSI for urban area classification," *IEEE Trans. Geosci. Remote Sens.*, vol. 53, no. 10, pp. 5312–5326, Oct 2015.

[6] W. Liao, J. Xia, P. Du, and W. Philips, "Semi-supervised graph fusion of hyperspectral and LiDAR data for classification," in *2015 IEEE International Geoscience and Remote Sensing Symposium (IGARSS)*, July 2015, pp. 53–56.

[7] J. Xia, L. Bombrun, T. Adali, Y. Berthoumieu, and C. Germain, "Classification of hyperspectral data with ensemble of subspace ICA and EPF," in *2016 IEEE International Conference on Acoustics, Speech and Signal Processing (ICASSP)*, March 2016, pp. 1422–1426.

[8] J. Castorena, U. S. Kamilov, and P. T. Boufounos, "Autocalibration of LiDAR and optical cameras via edge alignment," in *2016 IEEE International Conference on Acoustics, Speech and Signal Processing (ICASSP)*, March 2016, pp. 2862–2866.

[9] P. Ghamisi, B. Hfle, and X. X. Zhu, "Hyperspectral and lidar data fusion using extinction profiles and deep convolutional neural network," *IEEE J. Sel. Topics Appl. Earth Observ. Remote Sens.*, vol. 10, no. 6, pp. 3011–3024, June 2017.

[10] N. Kussul, M. Lavreniuk, S. Skakun, and A. Shelestov, "Deep learning classification of land cover and crop types using remote sensing data," *IEEE Geosci. Remote Sens. Lett.*, vol. 14, no. 5, pp. 778–782, May 2017.

[11] Yann Lecun, Yoshua Bengio, and Geoffrey Hinton, "Deep learning," vol. 521, pp. 436–444, 5 2015.

[12] L. Zhang, L. Zhang, and B. Du, "Deep learning for remote sensing data: A technical tutorial on the state of the art," *IEEE Geosci. Remote Sens. Mag.*, vol. 4, no. 2, pp. 22–40, June 2016.

[13] J Schmidhuber, "Deep learning in neural networks: An overview," *Neural Networks*, vol. 61, no. Supplement C, pp. 85 – 117, 2015.

[14] Z Zhou and J Feng, "Deep forest: Towards an alternative to deep neural networks," in *Proceedings of the Twenty-Sixth International Joint Conference on Artificial Intelligence (IJCAI)*, 2017, pp. 3553–3559.

[15] J. Xia, Z. Ming, and A. Iwasaki, "Multiple sources data fusion via deep forest," in *2018 IEEE International Geoscience and Remote Sensing Symposium (IGARSS)*, July 2017, pp. 1–4.

[16] Radhakrishna Achanta, Appu Shaji, Kevin Smith, Aurelien Lucchi, Pascal Fua, and Sabine Susstrunk, "Slic superpixels compared to state-of-the-art superpixel methods," *IEEE Trans. Pattern Anal. Mach. Intell.*, vol. 34, no. 11, pp. 2274–2282, Nov. 2012.

[17] W. Liao, R. Bellens, A. Pizurica, W. Philips, and Y. Pi, "Classification of hyperspectral data over urban areas using directional morphological profiles and semi-supervised feature extraction," *IEEE J. Sel. Topics Appl. Earth Observ. Remote Sens.*, vol. 5, no. 6, pp. 11771190, April 2012.

[18] B. Schölkopf, A. Smola, and K. Müller, "Nonlinear component analysis as a kernel eigenvalue problem," *Neural Comput.*, vol. 10, no. 5, pp. 1299–1319, July 1998.

[19] J. J. Rodriguez, L.I. Kuncheva, and C.J. Alonso, "Rotation forest: A new classifier ensemble method.," *IEEE Trans. Pattern Anal. Mach. Intell*, vol. 28, no. 10, pp. 1619–1630, 2006.

[20] J. Xia, J. Chanussot, P. Du, and X. He, "Spectral-spatial classification for hyperspectral data using rotation forests with local feature extraction and Markov random fields," *IEEE Trans. Geosci. Remote Sens.*, vol. 53, no. 5, pp. 2532–2546, 2015.

[21] W. Hu, Y. Huang, W. Li, F. Zhang, and H. Li, "Deep convolutional neural networks for hyperspectral image classification," *Journal of Sensors*, vol. 2015, Article ID: 258619, no. 9, 2015.